
The Autoencoding Variational Autoencoder

Taylan Cemgil
DeepMind
taylancemgil@google.com

Sumedh Ghaisas
DeepMind
sghaisas@google.com

Krishnamurthy Dvijotham
DeepMind
dvij@google.com

Sven Gowal
DeepMind
sgowal@google.com

Pushmeet Kohli
DeepMind
pushmeet@google.com

Abstract

Does a Variational AutoEncoder (VAE) consistently encode typical samples generated from its decoder? This paper shows that the perhaps surprising answer to this question is ‘No’; a (nominally trained) VAE does not necessarily amortize inference for typical samples that it is capable of generating. We study the implications of this behaviour on the learned representations and also the consequences of fixing it by introducing a notion of self consistency. Our approach hinges on an alternative construction of the variational approximation distribution to the true posterior of an extended VAE model with a Markov chain alternating between the encoder and the decoder. The method can be used to train a VAE model from scratch or given an already trained VAE, it can be run as a post processing step in an entirely self supervised way without access to the original training data. Our experimental analysis reveals that encoders trained with our self-consistency approach lead to representations that are robust (insensitive) to perturbations in the input introduced by adversarial attacks. We provide experimental results on the ColorMnist and CelebA benchmark datasets that quantify the properties of the learned representations and compare the approach with a baseline that is specifically trained for the desired property.

<https://github.com/deepmind/deepmind-research/tree/master/avae>

1 Introduction

The variational AutoEncoder (VAE) is a deep generative model [10, 15] where one can simultaneously learn a decoder and an encoder from data. An attractive feature of the VAE is that while it estimates an implicit density model for a given dataset via the decoder, it also provides an amortized inference procedure for computing a latent representation via the encoder. While learning a generative model for data, the decoder is the key object of interest. However, when the goal is extracting useful features from data and learning a good representation, the encoder plays a more central role [20]. In this paper, we will focus primarily on the encoder and its representation capabilities.

Learning good representations is one of the fundamental problems in machine learning to facilitate data-efficient learning and to boost the ability to transfer to new tasks. The surprising effectiveness of representation learning in various domains such as natural language processing [7] or computer vision [11] has motivated several research directions, in particular learning representations with desirable properties like adversarial robustness, disentanglement or compactness [1, 3–5, 12].

In this paper, our starting point is based on the assumption that if the learned decoder can provide a good approximation to the true data distribution, the exact posterior distribution (implied by the decoder) tends to possess many of the mentioned desired properties of a good representation, such as



Figure 1: Iteratively encoding and decoding a color MNIST image using a decoder and encoder (a) fitted a VAE with no observation noise (b) with AVAE. We find the drift in the generated images is an indicator of an inconsistency between the encoder and the decoder.

robustness. On a high level, we want to approximate properties of the exact posterior, in a way that supports representation learning.

One may naturally ask in what extent this goal is different from learning a standard VAE, where the encoder is doing amortized posterior inference and is directly approximating the true posterior. As we are using finite data for fitting within a restricted family of approximation distributions using local optimization, there will be a gap between the exact posterior and the variational approximation. We will illustrate that for finite data, even global minimization of the VAE objective is not sufficient to enforce natural properties which we would like a representation to have.

We identify the source of the problem as an inconsistency between the decoder and encoder, attributed to the lack of *autoencoding*, see also [2]. We argue that, from a probabilistic perspective, autoencoding for a VAE should ideally mean that samples generated by the decoder can be consistently encoded. More precisely, given any typical sample from the decoder model, the approximate conditional posterior over the latents should be concentrated on the values that could be used to generate the sample. In this paper, we show (through analysis and experiments) that this is not the case for a VAE learned with normal training and we propose an additional specification to enforce the model to autoencode, bringing us to the choice of the title of this paper.

Our Contributions: The key contributions of our work can be summarized as follows:

- We uncover that widely used VAE models are not autoencoding - samples generated by the decoder of a VAE are not mapped to the corresponding representations by the encoder, and an additional constraint on the approximating distribution is required.
- We derive a novel variational approach, Autoencoding VAE (AVAE), that is based on a new lower bound of the true marginal likelihood, and also enables data augmentation and self supervised density estimation in a theoretically principled way.
- We demonstrate that the learned representations achieve adversarial robustness. We show robustness of the learned representations in downstream classification tasks on two benchmark datasets: colorMNIST and CelebA. Our results suggest that a high performance can be achieved without adversarial training.

2 The Variational Autoencoder

The VAE is a latent variable model that has the form

$$Z \sim p(Z) = \mathcal{N}(Z; 0, I) \quad X|Z \sim p(X|Z, \theta) = \mathcal{N}(X; g(Z; \theta), vI) \quad (1)$$

where $\mathcal{N}(\cdot; \mu, \Sigma)$ denotes a Gaussian density with mean and covariance parameters μ and Σ , v is a positive scalar variance parameter and I is an identity matrix of suitable size. The mean function $g(Z; \theta)$ is parametrized typically by a deep neural network with parameters θ and the conditional distribution is known as the decoder. We use here a conditionally Gaussian observation model but other choices are possible, such as Bernoulli or Poisson, with mean parameters given by g .

To learn this model by maximum likelihood, one can use a variational approach to maximize the evidence lower bound (ELBO) defined as

$$\log p(X|\theta) \geq \langle \log p(X|Z, \theta) \rangle_{q(Z|X, \eta)} + \langle \log p(Z) \rangle_{q(Z|X, \eta)} + H[q(Z|X, \eta)] \equiv \mathcal{B}(\theta, \eta) \quad (2)$$

where $\langle h \rangle_q \equiv \int h(a)q(a)da$ denotes the expectation of the test function h with respect to the distribution q , and, H is the entropy functional $H[q] = -\langle \log q \rangle_q$. Here, q is an instrumental distribution, also known as the encoder, defined as

$$q(Z|X, \eta) = \mathcal{N}(Z; f^\mu(X; \eta), f^\Sigma(X; \eta))$$

Here, the functions f^μ and f^Σ are also chosen as deep neural networks with parameters η . Using the reparametrization trick [10], it is possible to optimize θ and η jointly by maximization of the ELBO using stochastic gradient descent aided by automatic differentiation. This mechanism is known as amortised inference, as once an encoder-decoder pair is trained, in principle the representation for a new data point can be readily calculated without the need of running a costly iterative inference procedure.

The ELBO in (2) is defined for a single data point X . It can be shown that in a batch setting, maximization of the ELBO is equivalent to minimization of the Kullback-Leibler divergence

$$\mathcal{KL}(\mathcal{Q}|\mathcal{P}) = \langle \log(\mathcal{Q}/\mathcal{P}) \rangle_{\mathcal{Q}} \quad \mathcal{Q} = \pi(X)q(Z|X, \eta) \quad \mathcal{P} = p(X|Z, \theta)p(Z) \quad (3)$$

with respect to θ and η . Here, π is ideally the true data distribution, but in practice it is replaced by the dataset, i.e., the empirical data distribution $\hat{\pi}(X) = \frac{1}{N} \sum_i \delta(X - x^{(i)})$. This form has also an intuitive interpretation as the minimization of the divergence between two alternative factorizations of a joint distribution with the desired marginals. See [21] for alternative interpretations of the ELBO including the one in (3). In the sequel, we will build our approach on this interpretation.

2.1 Extended VAE model for a pair of observations

In this section, we will justify the VAE from an alternative perspective of learning a variational approximation in an extended model, essentially first arriving at an identical algorithm to the original VAE. This alternative perspective enables us to justify additional specifications that a consistent encoder/decoder pair should satisfy.

Imagine the following extended VAE model for a pair of observations X, X'

$$(Z, Z') \sim p_\rho(Z, Z') = \mathcal{N} \left(\begin{pmatrix} Z \\ Z' \end{pmatrix}; \begin{pmatrix} 0 \\ 0 \end{pmatrix}, \begin{pmatrix} I & \rho I \\ \rho I & I \end{pmatrix} \right) \quad (4)$$

$$\begin{aligned} X|Z &\sim p(X|Z, \theta) = \mathcal{N}(X; g(Z; \theta), vI) \\ X'|Z' &\sim p(X'|Z', \theta) = \mathcal{N}(X'; g(Z'; \theta), vI) \end{aligned} \quad (5)$$

where the prior distribution $p_\rho(Z', Z)$ is chosen as symmetric with $p(Z') = p(Z)$, that is both marginals (here unit Gaussians) are equal in distribution. Here, I is the identity matrix and ρ is a hyperparameter $|\rho| \leq 1$ that we will refer as the coupling strength. Note that we have $p_\rho(Z'|Z) = \mathcal{N}(Z'; \rho Z, (1 - \rho^2)I)$. The two border cases $\rho = 1$ and $\rho = 0$, correspond to $Z' = Z$, and, independence $p(Z', Z) = p(Z')p(Z)$ respectively. This model defines the joint distribution

$$\bar{\mathcal{P}} \equiv p(X'|Z'; \theta)p(X|Z; \theta)p_\rho(Z', Z) \quad (6)$$

Proposition 2.1. *Approximating $\bar{\mathcal{P}}$ with a distribution of form*

$$\bar{\mathcal{Q}} \equiv \hat{\pi}(X)q(Z|X, \eta)p_\rho(Z'|Z)p(X'|Z', \theta) \quad (7)$$

where $\hat{\pi}$ is the empirical data distribution and q and p are the encoder and the decoder models respectively gives the original VAE objective in (3).

Proof: See Appendix A.1.

Proposition 2.1 shows that we could have derived the VAE from this extended model as well. This derivation is of course completely redundant since we introduce and cancel out terms. However, we will argue that this extended model is actually more relevant from a representation learning perspective where a coupling $\rho \approx 1$ is preferable as this is the desired behaviour of the encoder.

Example 2.1. Conditional Generation: Imagine that we generate a latent $z \sim p(Z)$ and an observation $x \sim p(X|Z = z; \theta)$ from the decoder of a VAE, but consequently discard z . Clearly, x is a sample from the marginal $p(X; \theta)$. Now suppose we are told to generate a new sample using the same z as $x' \sim p(X'|Z' = z; \theta)$. As we have discarded z , our best bet would be using the extended model with $\rho = 1$ and sample from $\bar{\mathcal{P}}(X'|X = x; \theta, \rho = 1)$ instead.

Example 2.2. Representation Learning: Imagine as in the previous example, that we generate a latent z and the corresponding observation x , but discard z . Suppose we are told to solve a classification task based on a classifier $p(y|z)$. As we have discarded z , we would ideally compute an expectation under the true posterior $\int p(y|Z)\bar{\mathcal{P}}(Z|X = x; \eta)dZ$. If our goal is learning the representation, and the task is unknown at training time, we wish to maintain as much as information about x . One strategy is asking a faithful reconstruction x' given x , i.e., we would like to be able to sample from $\bar{\mathcal{P}}(X'|X = x; \theta, \rho = 1)$ so the goal is not very different from conditional generation.

In practice, $\bar{\mathcal{P}}(X'|X = x; \theta, \rho)$ is not available and we would be using the approximate transition kernel $\bar{\mathcal{Q}}(X'|X; \cdot) \equiv \int \bar{\mathcal{Q}}dZdZ'/\hat{\pi}(X)$ obtained from the variational distribution. A natural question is how good the approximation $\bar{\mathcal{P}}(X'|X = x; \cdot) \approx \bar{\mathcal{Q}}(X'|X; \cdot)$ is for different ρ , and in particular $\rho \approx 1$. Therefore, we will investigate first some properties of this conditional distribution.

Proposition 2.2. *The marginal $\bar{\mathcal{P}}(X', X; \theta, \rho)$ is symmetric in X' and X , and its marginal does not depend on ρ , i.e., $\bar{\mathcal{P}}(X = x; \theta, \rho) = p(X; \theta)$ for any $|\rho| \leq 1$.*

Proof: See Appendix A.2.

The next proposition shows that if the encoder q is equal to the exact posterior, then $\bar{\mathcal{Q}}(X'|X; \cdot)$ is also exact

Proposition 2.3. *If the encoder q and decoder p satisfy the consistency condition*

$$q(Z|X, \eta)p(X; \theta) = p(X|Z; \theta)p(Z) \quad (8)$$

then, for all $|\rho| \leq 1$, we have $\bar{\mathcal{Q}}(X'|X; \cdot)p(X; \theta) = \bar{\mathcal{P}}(X', X; \theta, \rho)$. We will say that $\bar{\mathcal{Q}}(X'|X; \cdot)$ is $p(X; \theta)$ -invariant.

Proof: See Appendix A.3.

The subtle point of Proposition 2.3 is that the exact posterior is valid for any coupling strength parameter ρ . However, we have seen that the approximation computed by the VAE would be completely agnostic to our choice of ρ . Moreover, note that even if the original VAE objective is globally minimized to get $\mathcal{KL}(\hat{\pi}(X)q(Z|X, \eta)||p(X|Z, \theta)p(Z)) = 0$, this may not be sufficient to make sure that the transition kernel $\bar{\mathcal{Q}}(X'|X; \cdot)$ to be $p(X; \theta)$ -invariant. The empirical distribution $\hat{\pi}$ has a discrete support and we have no control over the encoder out of this support. Intuitively, we need to introduce additional terms to the objective to steer the encoder if we would like to use the model as a conditional generator, or as a representation especially in the regime $\rho \approx 1$. For this purpose, we will need to make our approximating distribution to match the transition $\bar{\mathcal{P}}(Z'|Z; \cdot) = p_\rho(Z'|Z)$ that is by construction $p(Z)$ invariant.

In Figure 1, we compare what can happen when a VAE is learned nominally with an example of expected behaviour. Here, we show a sequence of images generated by iteratively sampling from a nominally learned encoder-decoder pair on colorMNIST. The drift in the generated images points to a potential inconsistency between the decoder and the encoder. For further insight, we also discuss the special case of probabilistic PCA (Principal Component Analysis) in the appendix Section B, to give an analytically tractable example.

3 Autoencoding Variational Autoencoder (AAVE)

Motivated by our analysis, we propose using the following extended model as a target distribution,

$$\mathcal{P}_\rho = p(X|Z; \theta)p(Z)p_\rho(Z'|Z)u(\tilde{X}) \quad (9)$$

where ρ is considered as a fixed hyper-parameter, not to be learned from data. Here \tilde{X} is an additional auxiliary observation (a delusion) that we introduce. We want the target model to be agnostic to its value, hence we choose a flat distribution $u(\tilde{X}) = 1$. We choose as the approximating distribution

$$\mathcal{Q}_{AAVE} = q(Z'|\tilde{X}; \eta)p_\theta(\tilde{X}|Z)q(Z|X; \eta)\pi(X)$$

The central idea of AAVE is making the encoder and the decoder to be consistent both on the training data and on the auxiliary observations generated by the decoder. We use the notation p_θ to highlight that the decoder is considered as constant when used as a factor of \mathcal{Q}_{AAVE} otherwise the original VAE bound would be invalid. Intuitively, the self generated delusion \tilde{X} should not be changing the true log likelihood as otherwise we would be modifying the original objective. The following proposition justifies our choice:

Proposition 3.1. *Assume that the consistency condition (8) is true, Then, the transition kernel defined as*

$$\mathcal{Q}_{AAVE}(Z'|Z; \eta, \theta) \equiv \int q(Z'|\tilde{X}, \eta)p(\tilde{X}|Z; \theta)d\tilde{X}$$

is $p(Z)$ invariant. Moreover, assume that the latent space has a lower dimension than the observation space ($Z \in \mathbb{R}^{N_z}$ and $X \in \mathbb{R}^{N_x}$, and $N_z < N_x$), and the decoder mean mapping $g : \mathbb{R}^{N_z} \rightarrow \mathbb{X}_g$,

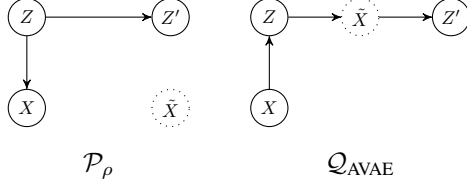


Figure 2: Graphical model of the extended target distribution \mathcal{P}_ρ , and the variational approximation $\mathcal{Q}_{\text{AVAE}}$. Here \tilde{X} is a sample generated by the decoder that is subsequently encoded by the encoder.

is one-to-one, where $\mathbb{X}_g \subset \mathbb{R}^{N_x}$ is the image of g . Then in the limit when the observation noise variance v goes to zero ($v \rightarrow 0$) we have $\mathcal{Q}_{\text{AVAE}}(Z'|Z; \eta, \theta) = p(Z'|Z; \rho = 1)$.

Proof: See Appendix A.4.

The proposition shows that our choice of the variational approximation (10) is natural: it forces $\mathcal{Q}_{\text{AVAE}}(Z', Z)$ to be close to the marginal of the exact posterior $\mathcal{P}(Z', Z) = p_\rho(Z'|Z)p(Z)$. The choice $\mathcal{Q}_{\text{AVAE}}$ is also convenient because it uses the original encoder and decoder as building blocks.

In the appendix Section C.1, we derive the variational objective $\mathcal{B}_{\text{AVAE}} = -\mathcal{KL}(\mathcal{Q}_{\text{AVAE}}||\mathcal{P}_\rho)$. The result is ¹

$$\begin{aligned} \mathcal{B}_{\text{AVAE}} = & + -\mathcal{KL}(\pi(X)q(Z|X; \eta)||p(X|Z; \theta)p(Z)) \\ & + \langle \log p_\rho(Z'|Z) \rangle_{\tilde{q}(Z; \eta)\tilde{q}_\theta(Z'|Z; \eta)} - \left\langle \log q(Z'|\tilde{X}; \eta) \right\rangle_{q(Z'|\tilde{X}; \eta)\tilde{q}_\theta(\tilde{X}; \eta)} \end{aligned} \quad (10)$$

where $\tilde{q}(Z; \eta) \equiv \int q(Z|X; \eta)\pi(X)dX$, $\tilde{q}_\theta(\tilde{X}; \eta) \equiv \int p_\theta(\tilde{X}|Z)\tilde{q}(Z; \eta)dZ$ and $\tilde{q}_\theta(Z'|Z; \eta) \equiv \int q(Z'|\tilde{X}; \eta)p_\theta(\tilde{X}|Z)d\tilde{X}$. In the appendix 1, we provide pseudocode with a stop-gradients primitive to avoid using contributions of θ dependent terms of \tilde{q}_θ to the gradient computation.

The resulting objective (10) is intuitive. The first term is identical to the standard VAE ELBO. The second term is a smoothness term that measures the distance between z (the representation that is used to generate the delusion) and z' (the encoding of the delusion). The third term is an extra entropy term on auxiliary observations.

3.1 Illustration

As a illustration, we show results for a discrete VAE, where both the encoder and the decoder can be represented as parametrized probability tables. Our goal in choosing a discrete model is visualization of the behaviour of the algorithms in a way that is independent from a particular neural network architecture. The details of this model are explained in the appendix Section D.

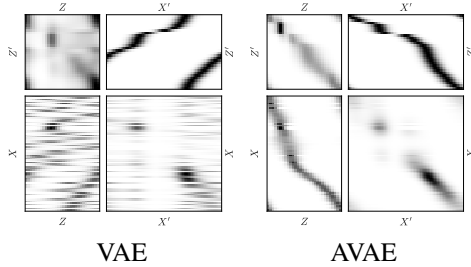


Figure 3: Each Panel is showing (from north east clockwise order) heatmaps of probabilities (darker is higher) i) the decoder $p(X'|Z'; \theta)$; ii) $\mathcal{Q}(X'|X; \theta, \eta)p(X; \theta)$; iii) the encoder $q(Z|X; \eta)$; iv) $\mathcal{Q}(Z|Z'; \theta, \eta)p(Z')$. See text for definitions.

We can visually compare the learned transition models of the learned encoders and decoders for VAE and AVAE in Figure 3, where we show for each model (starting from north east clockwise order) i) the estimated decoder $p(X'|Z'; \theta)$ (that is equal in distribution to $p(X|Z; \theta)$ due to parameter tying), ii) the joint distribution $\mathcal{Q}(X'|X; \theta, \eta)p(X; \theta)$, that should be ideally symmetric, where

$$\mathcal{Q}(X'|X; \theta, \eta) = \sum_z p(X'|Z' = z; \theta)q(Z = z|X; \eta)$$

with iii) the encoder $q(Z|X; \eta)$ and iv) the joint distribution $\mathcal{Q}(Z|Z'; \theta, \eta)p(Z')$ that should be also ideally symmetric and additionally should be close to identity where

$$\mathcal{Q}(Z|Z'; \theta, \eta) = \sum_x q(Z|X = x; \eta)p(X' = x|Z'; \theta).$$

¹When a and b are proportional, we write $\log a = + \log b$.

We see in Figure 3 that the joint distribution $Q(Z|Z';\theta,\eta)p(Z')$ is far from an identity mapping, and it is also not symmetrical. In contrast, the distributions learned by AVAE are enforced to be symmetrical, and the joint distribution is concentrated on the diagonal.

Intermediate summary: Learning a VAE from data is an highly ill-posed problem and regularization is necessary. Here, instead of modifying the decoder model, we have proposed to constrain the encoder in such a way that it approaches the desired properties of the exact posterior. Our argument started with the extended model in proposition 2.1 that admits the VAE as a marginal. In 2.2, we show that the exact decoder model is by construction independent of the choice of the coupling strength ρ . In plain language this means that, if we had access to the exact decoder and if we were able to do exact inference, any ρ will be acceptable. In this ideal case, the extended model would be actually redundant, and in 2.3, we highlight the properties of an exact encoder.

In practice however, we will be learning the decoder from data while doing only approximate amortized inference. Naturally, we want to still retain the properties of the exact posterior. We argue that the extended model is relevant for representation learning (see also example 2.2) and incorporate this explicitly to the encoder by AVAE, and in 3.1 we provide the justification that our choice coincides with the exact target conditional for $\rho = 1$, the representation learning case, when we encode and decode consistently.

We argue that encoder/decoder consistency is related to robustness. The existence of certain 'surprising' adversarial examples [17], where an input image is classified as a very different class after slightly changing input pixels, can be attributed non-smoothness of the representation such as having a large Lipschitz constant, see [5]. The smooth encoder (SE) method proposed in [5] attempted to fix this by data augmentation while training the encoder. In this paper, we introduce a more general framework, (where SE is also a special case) and investigate methods that circumvent the need for computationally costly adversarial attacks during training. The data augmentation is achieved by using the learned generative model itself, as a factor of the approximating Q_{AVAE} distribution. The AVAE objective ensures that samples that can be generated by the decoder in the vicinity of the representations corresponding to the training inputs are consistently encoded. In the next experimental section, we will show that the consistency translates to a nontrivial adversarial robustness performance. While our approach does not provide formal guarantees, learning an encoder that retains properties of an exact posterior seems to be central in achieving adversarial robustness.

4 Experimental Results

In this section, we will experimentally explore consequences of training with the AVAE objective in (10), implemented as Algorithm 1 in Appendix C. Optimizing the AVAE objective will change the learned encoder and decoder, and we expect that the additional terms will enforce a smooth representation leading to input perturbation robustness in downstream tasks. To test this claim, we will evaluate the encoder in terms of adversarial robustness, using an approach that will be described in the evaluation protocol. To see the effect of the new objective on the decoder and reconstruction quality, we will report Frechet Inception Distance (FID) [9], as well as the test mean square error (MSE).

Models: AVAE will be compared to two models, i) VAE trained using the standard ELBO (2), and, ii) Smooth Encoder (SE), a method recently proposed by [5] that uses the same target model as in (6), but uses a different variational approximation. This approximation is computed using adversarial attacks to generate the auxiliary observations \tilde{X} . We provide a self contained derivation of this algorithm in Appendix C.2. We also include two hybrid models in our simulations. iii) AVAE-SS (Self Supervised) a post-training method, where a VAE is first trained normally and then post-trained only by samples generated from the decoder (without training data, see Figure 4 for the graphical model – for details see appendix C.4). Finally, we also provide results for a model iv) SE-AVAE, a model that combines both the SE and the AVAE objectives and is concurrently trained using both adversarial attacks and self generated auxiliary observations (for details see appendix C.5). In all models, we use a latent space dimension of 64.

Data and Tasks: Experiments are conducted on datasets colorMNIST and CelebA, using both MLP and Convnet architectures in the former, and only Convnet in the latter (for details see Appendix F). The colorMNIST dataset has 2 separate downstream classification tasks (color, digit). For CelebA, we have 17 different binary classification tasks, such as ('has mustache?' or 'wearing hat?').

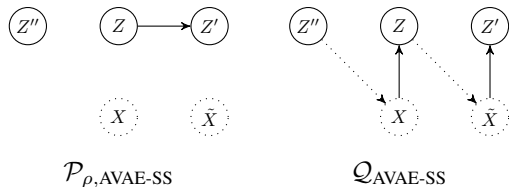


Figure 4: Graphical model of the AVAE-SS target distribution $\mathcal{P}_{\rho, \text{AVAE-SS}}$, and the variational approximation $\mathcal{Q}_{\text{AVAE-SS}}$. Here both X and \bar{X} is a sample generated by the decoder. The decoder factors (dotted arcs) is fixed (as pretrained by normal VAE).

Task	digit			color			Time	MSE	FID	
	ϵ	0.0	0.1	0.2	0.0	0.1				0.2
VAE		93.8	5.8	0.0	100.0	19.9	2.0	$\times 1$	1369.2	12.44
SE $_{0.1}^5$		94.3	89.6	1.8	100.0	100.0	21.8	$\times 4$	1372.5	13.01
SE $_{0.2}^5$		95.7	92.6	87.3	100.0	99.9	99.9	$\times 4$	1374.9	11.72
AVAE		97.3	88.1	54.8	100.0	99.8	87.7	$\times 1.5$	1371.9	15.46
SE $_{0.1}$ -AVAE		97.4	93.6	24.5	100.0	100.0	60.0	$\times 4.7$	1373.3	13.90
SE $_{0.2}$ -AVAE		97.6	94.2	79.8	100.0	100.0	83.2	$\times 4.7$	1374.3	13.89
AVAE SS		94.1	72.8	20.8	100.0	99.6	56.8	$\times 1.5$	1379.3	12.44

Table 1: Adversarial test accuracy (in percentage) of the representations for digit and color classification tasks on color MNIST (ConvNet). Evaluation attack radius is ϵ where pixels are normalized between $[0, 1]$. Time is the ratio of the wall-clock time of method to the time taken by the VAE. We show performance of the decoder in terms of MSE and FID score. For AVAE and SE, the coupling strengths are $\rho = 0.975$ and $\rho_{\text{SE}} = 0.95$. The subscript of SE $_{\epsilon'}$ is the radius ϵ' used during adversarial training of SE.

Evaluation Protocol: The learned representations will be evaluated by their robustness against adversarial perturbations. For the evaluation of adversarial accuracy we employ a three step process, i) first we train an encoder-decoder pair agnostic to any classification task, and ii) subsequently, we freeze the encoder parameters and use the mean mapping f^μ as a representation to train a linear classifier on top. Thus, each task specific classifier will share the common representation learned by the encoder. This linear classifier is trained normally, *without* any adversarial attacks. Finally, iii) we evaluate the adversarial accuracy of the resulting classifiers. For this, we compute an adversarial perturbation δ such that $\|\delta\|_\infty \leq \epsilon$ using projected gradient descent (PGD). Here, ϵ is the attack radius and the optimization goal is changing the classification decision to a different class. The adversarial accuracy is reported in terms of percentage of examples where the attack is not able to find an adversarial example.

Results: In Table 1, we show a comparison of the models on colorMNIST, where we evaluate adversarial accuracy for different attack radii ϵ (0.0 means no attack). Our key observation is that AVAE increases the nominal accuracy and achieves high adversarial robustness, that extends well to strong attacks with a large radius. The surprising fact is that the method is trained completely agnostic to the particular attack type (e.g, PGD), or the attack radius ϵ , and it is able to achieve comparable performance to SE. Due to the computational burden of adversarial attacks, a single iteration of SE takes almost 2.7 times more computation time than a single AVAE iteration, making AVAE practical for large networks. We also observe that for small ϵ , both objectives can be combined to provide improved adversarial accuracy (digit, $\epsilon = 0.1$), however, for higher radius ($\epsilon = 0.2$), the advantage seems to disappear. Another notable algorithm in Table 1 is AVAE-SS, where a pretrained VAE model can be further trained to significantly improve the robustness of the encoder. While this approach seems to be not competitive in terms of the final adversarial accuracy, the fact that it can improve robustness entirely in a self supervised way (Section C.4) is an attractive property.

In Figure 5, we show the summary of several experiments with different architectures, models and various choices of the coupling strength hyper-parameter ρ , on the colorMNIST dataset. The first column shows the effect of varying ρ , and as expected from our analysis, the adversarial accuracy is high for ρ close to one. The middle column compares different architectures in terms of training dynamics. For MLP, we see that adversarial accuracy slowly increases, while for Convnet, the improvement is very rapid. We also observe that AVAE-SS can significantly improve the robustness of a pretrained VAE, but not to the level of the other methods (results with further ρ are in Appendix G). The third column highlights the behaviour of the algorithms with increasing attack radius. We see

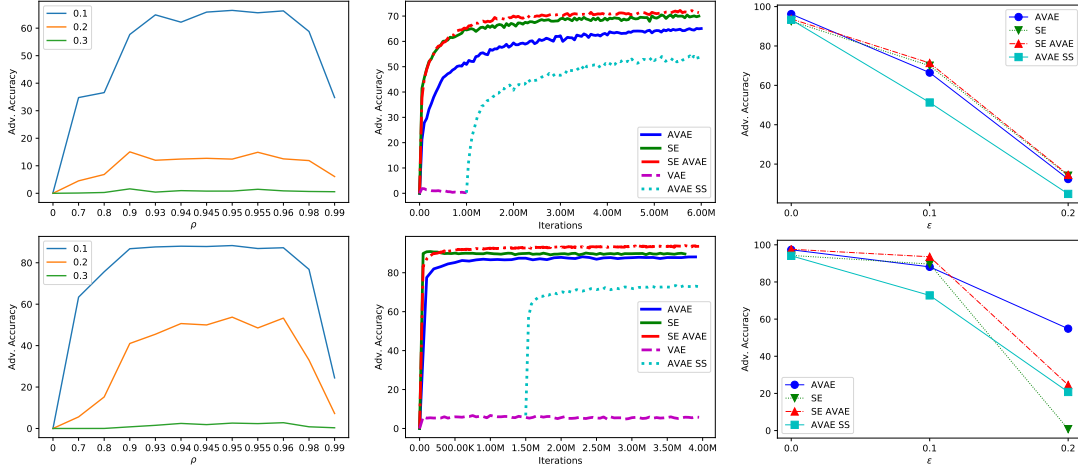


Figure 5: Adversarial accuracy of 'digit' classification task of colorMNIST. (Top row) All results use MLP architecture (Bottom row) Convnet architecture. (Left Column), Adversarial accuracy as a function of the coupling strength ρ for attack radius ϵ . (Middle column) Comparison of algorithms and test adversarial accuracy for attack radius $\epsilon = 0.1$, for $\rho = 0.975$ and $\rho_{SE} = 0.95$. (Right column) Adversarial accuracy as a function of the evaluation attack radius, SE model is trained with $\epsilon' = 0.1$ ($SE_{0.1}$).

Task / ϵ	AVAE		SE^5		SE^{20} [5]		SE^5 AVAE		AVAE SS	
	0.0	0.1	0.0	0.1	0.0	0.1	0.0	0.1	0.0	0.1
Bald	97.9	85.2	97.9	72.0	97.4	86.5	97.9	87.0	97.8	70.0
Mustache	96.1	91.5	95.0	69.5	95.7	84.4	96.0	92.3	94.9	74.3
Necklace	86.1	78.4	87.8	56.7	88.0	78.9	86.1	80.3	88.0	59.7
Eyeglasses	95.4	68.9	95.9	20.3	95.7	33.0	95.4	67.5	94.4	57.1
Smiling	77.7	3.6	87.0	3.10	85.7	1.1	77.9	6.3	81.4	0.9
Lipstick	81.0	7.3	83.9	2.0	80.3	0.6	80.2	11.5	80.7	0.9
Time	$\times 2.2$		$\times 3.1$		$\times 7.8$		$\times 4.3$		$\times 2.2$	
MSE	7276.6		7208.8		N/A		7269.2		7347.3	
FID	97.92		98.00		N/A		109.4		99.8	

Table 2: Adversarial test accuracy (in percentage) of the representations for subset of classification tasks on CelebA. For SE methods, superscript L in SE^L denotes the number of PGD iterations used during training of the model.

that for SE, the robustness does not extend beyond the radius that the model was trained for, whereas the accuracy of the AVAE trained model degrades gracefully.

In Table 2, we show that the robustness of a representation learned with AVAE extends to a complex dataset such as CelebA. The VAE results are omitted as they achieve around 0.0 adversarial accuracy and can be found in Table 3 in Appendix F, along with complete results on all tasks. We see that AVAE performs robustly in downstream tasks, and even surpasses robustness of SE^5 and even challenges SE^{20} (reported by [5]) which is substantially requires more computation. We observe that AVAE-SS also achieves non trivial adversarial accuracy across tasks, in some cases even beating SE^5 . Finally we also report results for SE-AVAE model, showing non-trivial improvements over both SE and AVAE model in most of the downstream tasks. Yet, the increased robustness seems to come with a cost: in all the experiments, we observe an increase in FID (lower is better) and MSE for AVAE models, indicating a tendency of reduced decoder quality and test set reconstruction. We conjecture that this tradeoff may be the result of the encoder being much more constrained than in the VAE case.

5 Conclusions

We show that VAE models derived from the canonical formulation in (1) are not unique. We used an alternative model (5) to show that the standard model is unable to capture some desired properties of the exact posterior that are important for representation learning. We proposed a principled alternative, the AVAE, and observed that it gives rise to robust representations without requiring adversarial training. In addition, we present a self supervised variant (AVAE-SS) that also exhibits robustness.

The paper justifies, theoretically and experimentally, the modelling choices of AVAE. Using two benchmark datasets, we demonstrate that the approach can achieve surprisingly high adversarial accuracy without adversarial training. An important feature of the AVAE is that the likelihood function is still equal to the standard VAE likelihood. In doing so, we also provide a principled justification for data augmentation in a density estimation context, where naive data augmentation is not valid as it alters the data distribution. In our framework, the generated data points act like nuisance parameters of the approximating distribution and do not have an effect on the estimated decoder.

Although we are not modifying the original likelihood function, currently, we observe a tradeoff: while the learnt encoder becomes more robust, the corresponding decoder seems to slightly suffer in quality, as measured by FID and MSE. It remains to be seen if there is actually a fundamental reason behind this and we believe that with more carefully designed training methods, both the decoder and the encoder could be in principle improved.

The autoencoding specification is related loosely to the concept of *cycle consistency*, that is often enforced between two data modalities [22]. In [8], authors propose a supervised VAE model for pairs of data points with the same labels to enforce disentanglement by using extra relational information (similar relational models include [18, 13]). In contrast, our approach does only change the encoder. Our method is a VAE based representation learning approach, and there is a large literature on the subject, see, e.g. [20], however models are often not evaluated on their robustness properties. Another fruitful approach in representation learning, especially for the image modality, is contrastive learning [14, 6]. These approaches can challenge and surpass supervised approaches in terms of label efficiency and accuracy, and it remains a future work to investigate the links with our work and whether or not these models can also be used for learning robust representations.

6 Societal Impact

General Research Direction. In recent years, researchers have trained deep generative models that can generate synthetic examples, often indistinguishable from natural data. The high quality of these samples suggest that these models may be able to learn latent representations useful for other downstream tasks. Learning such representations without task specific supervision facilitates transfer to yet unseen, future tasks. This also fosters label efficiency, and interpretability. Unsupervised representation learning would have a high societal impact as it could enable learning representations from data that can be shared with a wider community of researchers who do not have the computational resources for training such a representations, or do not have direct access to training data due to privacy/security/commercial considerations. However, the properties of these representations in terms of test accuracy, robustness, privacy preservation must be carefully studied before their release, especially if systems will be deployed in the real world. In the current work, we have taken a step towards learning representations in an unsupervised way, that exhibit robustness against transformations of the input.

Ethical Considerations. The current work studies representations learned by a specific generative model, the VAE and shares a finding that training a VAE by enforcing an additional natural autoencoding specification is able to provide significant robustness on the learned representation without adversarial training. The study is not proposing a particular system for a specific application. The human face dataset CelebA is chosen as a standard benchmark dataset with several attributes to illustrate the viability of the approach. Still, we have decided to exclude potentially sensitive and subjective attributes from the original dataset, such as 'big-nose' or 'Asian', and use only 17 neutral attributes that we have selected using our own judgment.

Acknowledgments and Disclosure of Funding

We would like to thank Andriy Minh for the fruitful discussions and excellent feedback.

References

- [1] Alessandro Achille and Stefano Soatto. Emergence of invariance and disentanglement in deep representations. *The Journal of Machine Learning Research*, 19(1):1947–1980, 2018.
- [2] Guillaume Alain and Yoshua Bengio. What regularized auto-encoders learn from the data-generating distribution. *J. Mach. Learn. Res.*, 15(1):3563–3593, January 2014.
- [3] Yoshua Bengio. Deep learning of representations for unsupervised and transfer learning. In *Proceedings of ICML workshop on unsupervised and transfer learning*, pages 17–36, 2012.
- [4] Christopher P. Burgess, Irina Higgins, Arka Pal, Loic Matthey, Nick Watters, Guillaume Desjardins, and Alexander Lerchner. Understanding disentangling in β -VAE. *arXiv e-prints*, page arXiv:1804.03599, Apr 2018.
- [5] A. T. Cemgil, S. Ghaisas, K. Dvijotham, and P. Kohli. Adversarially robust representations with smooth encoders. In *Proceedings of the Eighth International Conference on Learning Representations*, ICLR 2020, 2020.
- [6] Ting Chen, Simon Kornblith, Mohammad Norouzi, and Geoffrey Hinton. A simple framework for contrastive learning of visual representations. In *International Conference on Machine Learning*, 2020.
- [7] Jacob Devlin, Ming-Wei Chang, Kenton Lee, and Kristina Toutanova. Bert: Pre-training of deep bidirectional transformers for language understanding, 2018.
- [8] Ananya Harsh Jha, Saket Anand, Maneesh Singh, and VSR Veeravasarapu. Disentangling factors of variation with cycle-consistent variational auto-encoders. In *Proceedings of the European Conference on Computer Vision (ECCV)*, pages 805–820, 2018.
- [9] Martin Heusel, Hubert Ramsauer, Thomas Unterthiner, Bernhard Nessler, and Sepp Hochreiter. Gans trained by a two time-scale update rule converge to a local nash equilibrium. In *Proceedings of the 31st International Conference on Neural Information Processing Systems, NIPS’17*, page 6629–6640, Red Hook, NY, USA, 2017. Curran Associates Inc.
- [10] Diederik P. Kingma and Max Welling. Auto-encoding variational bayes. In Yoshua Bengio and Yann LeCun, editors, *2nd International Conference on Learning Representations, ICLR 2014, Banff, AB, Canada, April 14-16, 2014, Conference Track Proceedings*, 2014.
- [11] Alex Krizhevsky, Ilya Sutskever, and Geoffrey E Hinton. Imagenet classification with deep convolutional neural networks. In F. Pereira, C. J. C. Burges, L. Bottou, and K. Q. Weinberger, editors, *Advances in Neural Information Processing Systems 25*, pages 1097–1105. Curran Associates, Inc., 2012.
- [12] Francesco Locatello, Stefan Bauer, Mario Lucic, Gunnar Raetsch, Sylvain Gelly, Bernhard Schölkopf, and Olivier Bachem. Challenging common assumptions in the unsupervised learning of disentangled representations. In Kamalika Chaudhuri and Ruslan Salakhutdinov, editors, *Proceedings of the 36th International Conference on Machine Learning*, volume 97 of *Proceedings of Machine Learning Research*, pages 4114–4124, Long Beach, California, USA, 09–15 Jun 2019. PMLR.
- [13] Christos Louizos, Xiahn Shi, Klamer Schutte, and Max Welling. The Functional Neural Process. *arXiv e-prints*, page arXiv:1906.08324, Jun 2019.
- [14] Aaron van den Oord, Yazhe Li, and Oriol Vinyals. Representation learning with contrastive predictive coding. *arXiv preprint arXiv:1807.03748*, 2018.

- [15] Danilo Jimenez Rezende, Shakir Mohamed, and Daan Wierstra. Stochastic backpropagation and approximate inference in deep generative models. In Eric P. Xing and Tony Jebara, editors, *Proceedings of the 31st International Conference on Machine Learning*, volume 32 of *Proceedings of Machine Learning Research*, pages 1278–1286, Beijing, China, 22–24 Jun 2014. PMLR.
- [16] Sam T Roweis. Em algorithms for pca and spca. In *Advances in neural information processing systems*, pages 626–632, 1998.
- [17] Christian Szegedy, Wojciech Zaremba, Ilya Sutskever, Joan Bruna, Dumitru Erhan, Ian Goodfellow, and Rob Fergus. Intriguing properties of neural networks. *arXiv preprint arXiv:1312.6199*, 2013.
- [18] Da Tang, Dawen Liang, Tony Jebara, and Nicholas Ruozzi. Correlated Variational Auto-Encoders. *arXiv e-prints*, page arXiv:1905.05335, May 2019.
- [19] Michael E. Tipping and Christopher M. Bishop. Probabilistic principal component analysis. *Journal of the Royal Statistical Society: Series B (Statistical Methodology)*, 61(3):611–622, 1999.
- [20] Michael Tschannen, Olivier Bachem, and Mario Lucic. Recent advances in autoencoder-based representation learning. In *Third workshop on Bayesian Deep Learning (NeurIPS 2018)*, 2018.
- [21] Shengjia Zhao, Jiaming Song, and Stefano Ermon. Infovae: Balancing learning and inference in variational autoencoders. In *Proceedings of the AAAI Conference on Artificial Intelligence*, volume 33, pages 5885–5892, 2019.
- [22] Jun-Yan Zhu, Taesung Park, Phillip Isola, and Alexei A Efros. Unpaired image-to-image translation using cycle-consistent adversarial networks. In *Proceedings of the IEEE international conference on computer vision*, pages 2223–2232, 2017.

A Proofs

In this section, we provide the proofs of the propositions stated in the main text.

A.1 Proposition 2.1

Proof. By definition

$$\mathcal{KL}(\bar{\mathcal{Q}}|\bar{\mathcal{P}}) = - \left\langle \log \frac{p(X|Z; \theta)p(Z)p_\rho(Z'|Z)p(X'|Z'; \theta)}{\hat{\pi}(X)q(Z|X, \eta)p_\rho(Z'|Z)p(X'|Z', \theta)} \right\rangle_{\bar{\mathcal{Q}}} = \mathcal{KL}(\mathcal{Q}|\mathcal{P})$$

Equality follows as for any test function of form $f(X, Z)$, that does not depend on X' and Z' we have $\langle f(X, Z) \rangle_{\bar{\mathcal{Q}}} = \langle f(X, Z) \rangle_{\mathcal{Q}}$. \square

A.2 Proposition 2.2

Proof. $\bar{\mathcal{P}}$ is symmetric (exchangeable) in (X', Z') and (X, Z) . Hence, the pairwise marginal

$$\bar{\mathcal{P}}(X', X; \theta, \rho) = \int \bar{\mathcal{P}}(X, X', Z, Z'; \theta, \rho) dZ dZ' \quad (11)$$

is also symmetric by the parametrization, and X' and X are exchangeable with identical marginal densities. We have $\bar{\mathcal{P}}(X; \theta, \rho) = p(X; \theta)$ as the marginals of $p_\rho(Z', Z)$ do not depend on ρ . Hence we have $\bar{\mathcal{P}}(X'|X = x; \theta, \rho) = \bar{\mathcal{P}}(X', X; \theta, \rho)/p(X; \theta)$. \square

A.3 Proposition 2.3

Proof. Consider the joint distribution

$$\begin{aligned} \bar{\mathcal{Q}}(X'|X; \eta, \theta, \rho)p(X; \theta) &= \int (q(Z|X, \eta)p(X; \theta)) p_\rho(Z'|Z)p(X'|Z', \theta) dZ dZ' \\ &= \int p(X|Z; \theta)p(Z)p_\rho(Z'|Z)p(X'|Z', \theta) dZ dZ' = \bar{\mathcal{P}}(X, X'; \theta, \rho) \end{aligned}$$

The invariance of $p(X; \theta)$ follows from symmetry as $\int \bar{\mathcal{Q}}(X'|X; \cdot)p(X; \theta) = p(X'; \theta)$. \square

A.4 Proposition 3.1

Proof. Consider

$$\mathcal{Q}_{\text{AVAE}}(Z'|Z; \eta, \theta)p(Z) \equiv \int q(Z'|\tilde{X}, \eta)p(\tilde{X}|Z; \theta)p(Z)d\tilde{X} = \int q(Z'|\tilde{X}, \eta)q(Z|\tilde{X}, \eta)p(\tilde{X}; \theta)d\tilde{X}$$

As the expression at the right is symmetric in Z and Z' , $p(Z)$ -invariance follows. When the observation noise $v \rightarrow 0$, the probability of observing \tilde{x} out of the image of g vanishes, i.e., $\Pr\{\tilde{x} \notin \mathbb{X}_g\} = 0$. When g is continuous and differentiable, the image of g is a manifold \mathbb{X}_g . As g is one-to-one, it is invertible on \mathbb{X}_g , $\tilde{x} = g(z; \theta) \Leftrightarrow g^{-1}(\tilde{x}) = z$ and the optimal encoder will have the mean mapping $f^\mu(\tilde{x}; \eta^*) = g^{-1}(\tilde{x}; \eta^*)$ and variance mapping $f^\Sigma(\tilde{x}; \eta^*) = 0$. As $z' = g^{-1}(\tilde{x})$ and $\tilde{x} = g(z)$, we have $z' = z$ and have $\mathcal{Q}_{\text{AVAE}}(Z'|Z; \eta, \theta) = p(Z'|Z; \rho = 1)$. \square

B Example: PCA case

As a special case, it is informative to consider the probabilistic principal component analysis (pPCA) [16, 19], a special case of VAE where g and f^μ are constrained to be linear functions. When $g(Z; \theta = W) = Wz$, using standard results about Gaussian distributions, the optimal encoder is given by the exact posterior and is available in closed form as

$$q_*(Z|X = x) = \mathcal{N}(Z; f_*^\mu(x), f_*^\Sigma)$$

where $f_*^\mu(x) = (W^\top W + vI)^{-1}W^\top x$, $f_*^\Sigma = v(W^\top W + vI)^{-1}$. The transition kernel can be shown to be the following form

$$\mathcal{Q}(X'|X = x) = \mathcal{N}(X'; P_{W,v}x, v(P_{W,v} + I))$$

where $P_{W,v} = W(W^\top W + vI)^{-1}W^\top$.

In the limit when v is zero, we have the PCA case and the mean mapping of the transition kernel $g \circ f_*^\mu$ corresponds to a projection matrix $P_{W,0} = P_W = W(W^\top W)^{-1}W^\top$, as $P_W = P_W^2$. Hence all noise will vanish, and iterating the encode-decode steps would generate the sequence $P_W x_0 = x_1 = x_2 = \dots$; any initial input will be projected first into the range space of the projector, and subsequent points will be confined to the invariant subspace.

Note that the encoder and the decoder are also consistent, as any possible sample x that can be generated by the decoder, is mapped to a representation in the vicinity of the original representation. To see this, consider the transition kernel that can be shown to be

$$\mathcal{Q}(Z'|Z = z) = \mathcal{N}(Z'; J_{W,v}z, S)$$

where $J_{W,v} = (W^\top W + vI)^{-1}W^\top W$ and $S = v(J_{W,v} + I)(W^\top W + vI)^{-1}$. In the limit, when v goes to zero, we have $J_{W,v} \approx I$, or equivalently $z' = z$.

However, if an 'inconsistent' decoder-encoder pair would be used, an encoder with a perturbed mean transform $(W^\top W + vI)^{-1}W^\top + \Delta$ for some nonzero matrix Δ , the resulting transition matrix of $\mathcal{Q}(X'|X = x)$ won't be in general a projection and the chains will 'drift away' from the original invariant subspace depending upon the norm of the perturbation and the spectrum of the resulting matrix $W\Delta$.

In the PCA case, the invariant subspace is explicitly known thanks to the linearity. In contrast, for a VAE with flexible nonlinear decoder and encoder functions, the analogous object to an invariant subspace would be a global invariant manifold (sometimes referred as the data manifold), embedded in \mathcal{X} and each manifold point charted by $x = g(z; \theta)$ where z is the coordinate of x in \mathcal{Z} , given by $f^\mu(x)$. While it seems to be hard to characterize the invariant manifold, we can argue that "autoencoding" requires that realizations generated by the decoder are approximately invariant when encoded again; i.e. autoencoding means that the coordinate of the point $g(z)$ is z , or equivalently $z \approx f^\mu(g(z))$. However, this requirement is enforced by the VAE only for the samples in the dataset but not for typical samples z from the prior $p(Z)$. So the name autoencoder is perhaps a misnomer as the resulting model is not necessarily autoencoding the samples it can generate.

C Variational Approximations

In this appendix, we provide the derivation of the variational objective for the AVAE and then an alternative derivation for the smooth encoder [5], and other hybrid models that we used in our experiments as contender models.

C.1 Autoencoding Variational Autoencoder $\mathcal{Q}_{\text{AVAE}}$

The AVAE objective is

$$(\theta^*, \eta^*) = \arg \max_{\theta, \eta} \mathcal{B}_{\text{AVAE}}(\theta, \eta)$$

where

$$\mathcal{B}_{\text{AVAE}}(\theta, \eta) = -\mathcal{KL}(\mathcal{Q}_{\text{AVAE}}|\mathcal{P}_\rho) = \langle \log(\mathcal{P}_\rho/\mathcal{Q}_{\text{AVAE}}) \rangle_{\mathcal{Q}_{\text{AVAE}}}$$

The target distribution is

$$\mathcal{P}_\rho = p(X|Z; \theta)p(Z)p_\rho(Z'|Z)u(\tilde{X}) \quad (12)$$

where ρ is considered as a fixed hyper-parameter and $u(\tilde{x}) = 1$. The approximating distribution is

$$\begin{aligned} \mathcal{Q}_{\text{AVAE}} &= \pi(X)q(Z|X; \eta)q(Z'|\tilde{X}; \eta)p_\theta(\tilde{X}|Z) \\ \mathcal{B}_{\text{AVAE}}(\theta, \eta) &= \left\langle \log \frac{p(X|Z; \theta)p(Z)p_\rho(Z'|Z)u(\tilde{X})}{\pi(X)q(Z|X; \eta)q(Z'|\tilde{X}; \eta)p_\theta(\tilde{X}|Z)} \right\rangle_{\mathcal{Q}_{\text{AVAE}}} \\ &= -\mathcal{KL}(\pi(X)q(Z|X; \eta)|p(X|Z; \theta)p(Z)) \\ &\quad + \left\langle \log \frac{p_\rho(Z'|Z)}{q(Z'|\tilde{X}; \eta)p_\theta(\tilde{X}|Z)} \right\rangle_{\tilde{q}(Z; \eta)q(Z'|\tilde{X}; \eta)p_\theta(\tilde{X}|Z)} \end{aligned}$$

We have used p_θ in the subscript to denote the fact that the decoder parameters will be assumed to be fixed. Cancelling the constant terms we obtain

$$\begin{aligned} \mathcal{B}_{\text{AVAE}} = & + \langle \log p(X|Z; \theta) \rangle_{\pi(X)q(Z|X; \eta)} + \langle \log p(Z) \rangle_{\pi(X)q(Z|X; \eta)} - \langle \log q(Z|X; \eta) \rangle_{\pi(X)q(Z|X; \eta)} \\ & + \langle \log p(Z'|Z; \rho) \rangle_{\tilde{q}(Z; \eta)\tilde{q}(Z'|Z; \eta)} - \langle \log q(Z'|\tilde{X}; \eta) \rangle_{q(Z'|\tilde{X}; \eta)\tilde{q}(\tilde{X}; \eta)} \end{aligned}$$

where $\tilde{q}_\theta(Z'|Z; \eta) \equiv \int q(Z'|\tilde{X}; \eta)p_\theta(\tilde{X}|Z)d\tilde{X}$, $\tilde{q}(\tilde{X}; \eta) \equiv \int q(\tilde{X}|X; \eta)\pi(X)dX$ and $\tilde{q}(Z; \eta) \equiv \int q(Z|X; \eta)\pi(X)dX$.

The algorithm is shown in Algorithm 1. We approximate the required expectations by their Monte Carlo estimates and the objective function to maximize becomes

$$\begin{aligned} \hat{\mathcal{B}}_{\text{AVAE}}(\theta, \eta; x, \tilde{x}, z) = & \log p(X = x|Z = z; \theta) \\ & + \langle \log p(Z) \rangle_{q(Z|X=x; \eta)} + \langle \log p(Z'|Z; \rho) \rangle_{\tilde{q}(Z|X=x; \eta)\tilde{q}(Z'|\tilde{X}=\tilde{x}; \eta)} \\ & - \langle \log q(Z'|\tilde{X} = \tilde{x}; \eta) \rangle_{q(Z'|\tilde{X}=\tilde{x}; \eta)} \\ & - \langle \log q(Z|X = x; \eta) \rangle_{q(Z|X=x; \eta)} \end{aligned} \quad (13)$$

Algorithm 1: AVAE Training	Algorithm 2: SE Training
<pre> 1: function TRAINAVAE(x, iterations) 2: encoder $\leftarrow (f^\mu(\cdot; \eta), f^\Sigma(\cdot; \eta))$ 3: decoder $\leftarrow g(\cdot; \theta)$ 4: for $i \leftarrow 1$ to iterations do 5: $\mu_x, \Sigma_x^{1/2} \leftarrow \text{encoder}(x)$ 6: $z \leftarrow \mu_x + \Sigma_x^{1/2} \mathcal{N}(0, 1)$ 7: $\tilde{x} \leftarrow \text{stopgradient}(\text{decoder}(z))$ 8: $\mu_{\tilde{x}}, \Sigma_{\tilde{x}}^{1/2} \leftarrow \text{encoder}(\tilde{x})$ 9: Maximize$_{\theta, \eta} \hat{\mathcal{B}}_{\text{AVAE}}(\theta, \eta; x, \tilde{x}, z)$ ▷ See (13) 10: end for 11: end function </pre>	<pre> 1: function TRAINSE(x, iterations) 2: encoder $\leftarrow (f^\mu(\cdot; \eta), f^\Sigma(\cdot; \eta))$ 3: decoder $\leftarrow g(\cdot; \theta)$ 4: for $i \leftarrow 1$ to iterations do 5: $\tilde{x} \leftarrow \text{stopgradient}(\text{PGD}(x))$ 6: $\mu_x, \Sigma_x^{1/2} \leftarrow \text{encoder}(x)$ 7: $z \leftarrow \mu_x + \Sigma_x^{1/2} \mathcal{N}(0, 1)$ 8: Maximize$_{\theta, \eta} \hat{\mathcal{B}}_{\text{SE}}(\theta, \eta; x, \tilde{x}, z)$ ▷ See (32) 9: end for 10: end function </pre>
Algorithm 3: SE-AVAE Training	Algorithm 4: AVAE-SS Training
<pre> 1: function TRAINSE-AVAE(x, iterations) 2: encoder $\leftarrow (f^\mu(\cdot; \eta), f^\Sigma(\cdot; \eta))$ 3: decoder $\leftarrow g(\cdot; \theta)$ 4: for $i \leftarrow 1$ to iterations do 5: $\tilde{x} \leftarrow \text{stopgradient}(\text{PGD}(x))$ 6: $\mu_x, \Sigma_x^{1/2} \leftarrow \text{encoder}(x)$ 7: $z \leftarrow \mu_x + \Sigma_x^{1/2} \mathcal{N}(0, 1)$ 8: $\tilde{x} \leftarrow \text{stopgradient}(\text{decoder}(z))$ 9: Maximize$_{\theta, \eta} \hat{\mathcal{B}}_{\text{SE-AVAE}}(\theta, \eta; x, \tilde{x}, \tilde{x}, z)$ ▷ See (35) 10: end for 11: end function </pre>	<pre> 1: function TRAINAVAE-SS(x, iterations) 2: encoder $\leftarrow (f^\mu(\cdot; \eta), f^\Sigma(\cdot; \eta))$ 3: decoder $\leftarrow g(\cdot; \theta)$ 4: for $i \leftarrow 1$ to iterations do 5: $z'' \leftarrow \mathcal{N}(0, 1)$ 6: $x \leftarrow \text{stopgradient}(\text{decoder}(z''))$ 7: $\mu_x, \Sigma_x^{1/2} \leftarrow \text{encoder}(x)$ 8: $z \leftarrow \mu_x + \Sigma_x^{1/2} \mathcal{N}(0, 1)$ 9: $\tilde{x} \leftarrow \text{stopgradient}(\text{decoder}(z))$ 10: Maximize$_{\theta, \eta} \hat{\mathcal{B}}_{\text{AVAE-SS}}(\theta, \eta; x, \tilde{x}, z)$ ▷ See (34) 11: end for 12: end function </pre>

C.2 Smooth Encoder

Smooth encoder model proposed in [5] employs an alternative variational approximation strategy to learn a representation. While SE introduced an ‘external selection mechanism’ to generate adversarial examples, the analysis in this appendix shows that the approach could be viewed as a robust Bayesian approach to variational inference and choosing a different variational distribution than AVAE.

SE aims at learning a model that is insensitive to a class of input transformations, in particular small input perturbations $T_\alpha(x) = x + \alpha$ where $\alpha \in A = \{\alpha : \|\alpha\| \leq \epsilon\}$. The variational distribution has the form

$$\mathcal{Q}_{\text{SE}} = \pi(X)q(Z|X; \eta)q_T(\tilde{X}|X; u_A)q(Z'|\tilde{X}; \eta) \quad (14)$$

where $q_T(\tilde{X}|X; u_A)$ is the conditional distribution defined by

$$\alpha \sim u_A(\alpha) \quad \tilde{X} = T_\alpha(X) \quad (15)$$

Here, u_A is an arbitrary distribution with $u_A \in \mathcal{U}_A$, where \mathcal{U}_A is the set of distributions defined on A . The notation suggests that u_A is now taken as a parameter. The bound is

$$\tilde{\mathcal{B}}_{\text{SE}}(\eta, \theta; u_A) = -\mathcal{KL}(\mathcal{Q}_{\text{SE}}(\eta, u_A) \parallel \mathcal{P}_\rho(\theta)) \quad (16)$$

We can employ a robust Bayesian approach to define a ‘pessimistic’ bound in the sense of selecting the worst prior distribution u_A

$$\mathcal{B}_{\text{SE}}(\eta, \theta) = \min_{u_A \in \mathcal{U}_A} \tilde{\mathcal{B}}_{\text{SE}}(\eta, \theta; u_A) \quad (17)$$

This optimization is still computationally feasible as the maximum will be attained by a degenerate distribution concentrated on an adversarial example $x_a = x + \alpha$ as $u_A(\alpha) = \delta(\alpha - (x_a - x))$ and can be computed using projected gradient descent to find x_a . Once u_A is fixed, we can optimize model parameters in the outer maximization.

The resulting algorithm has two steps i) (Augmentation) Generate a new empirical data distribution $\hat{\pi}_a(\tilde{X}|X)$ adversarially, by finding the worst case transformation for each data point in the sense of maximizing the change between representations; and ii) (Maximization) Maximizing the bound denoted by \mathcal{B}_{SE} that has the following form

$$\mathcal{B}_{\text{SE}} = + \langle \log p(X|Z; \theta) \rangle_{\pi(X)q(Z|X; \eta)} - \mathcal{KL}(\tilde{\pi}_a(X, \tilde{X})q(Z, Z'|X, \tilde{X}; \eta) \parallel p(Z, Z'; \rho)) \quad (18)$$

where $q(Z, Z'|X, \tilde{X}; \eta) \equiv q(Z|X; \eta)q(Z'|\tilde{X}; \eta)$ and $\tilde{\pi}_a(X, \tilde{X}) \equiv \pi(X)\hat{\pi}_a(\tilde{X}|X)$.

This objective measures the data fidelity (first term) and the divergence of the joint encoder mapping from the pairwise coupling target (second term). The second term forces the encoder mapping to be smooth when $\rho \approx 1$.

C.3 Derivation Details

- The SE objective:

$$(\theta^*, \eta^*) = \arg \max_{\theta, \eta} \min_{u_A \in \mathcal{U}_A} \tilde{\mathcal{B}}_{\text{SE}}(\theta, \eta; u_A)$$

$$\tilde{\mathcal{B}}_{\text{SE}}(\theta, \eta; u_A) = -\mathcal{KL}(\mathcal{Q}_{\text{SE}}(\eta; u_A) \parallel \mathcal{P}_\rho(\theta)) = \langle \log(\mathcal{P}_\rho / \mathcal{Q}_{\text{SE}}) \rangle_{\mathcal{Q}_{\text{SE}}}$$

- Target:

$$\mathcal{P}_\rho = p(X|Z; \theta)p(Z)p_\rho(Z'|Z)u(\tilde{X}) \quad (19)$$

fixed hyper-parameter $\rho \in [0, 1)$ and $u(\tilde{x}) = 1$.

- The variational distribution:

$$\mathcal{Q}_{\text{SE}}(\eta; u_A) = \pi(X)q(Z|X; \eta)q_T(\tilde{X}|X; u_A)q(Z'|\tilde{X}; \eta) \quad (20)$$

- $\pi(X)$: Data distribution to be replaced by empirical data distribution
- $q(Z|X; \eta), q(Z'|\tilde{X}; \eta)$: Encoders tied with same parameters η

– $q_T(\tilde{X}|X; u_A)$: Distribution induced by random translations

$$\alpha \sim u_A(\alpha) \quad \tilde{X} = X + \alpha \quad (21)$$

Here, u_A is an arbitrary distribution on $A = \{a : \|a\|_\infty \leq \epsilon\}$ with $u_A \in \mathcal{U}_A$.

$$\begin{aligned} \tilde{\mathcal{B}}_{\text{SE}}(\theta, \eta; u_A) &=^+ \langle \log p(X|Z; \theta) p(Z) p_\rho(Z'|Z) \rangle_{\mathcal{Q}_{\text{SE}}} \\ &\quad - \left\langle \log q(Z|X; \eta) q(Z'|\tilde{X}; \eta) \right\rangle_{\mathcal{Q}_{\text{SE}}} - \left\langle \log q_T(\tilde{X}|X; u_A) \right\rangle_{\mathcal{Q}_{\text{SE}}} \quad (22) \\ &= \langle \log p(X|Z; \theta) \rangle_{\pi(X)q(Z|X; \eta)} \\ &\quad + \langle \log p(Z) \rangle_{\pi(X)q(Z|X; \eta)} \\ &\quad - \langle \log q(Z|X; \eta) \rangle_{\pi(X)q(Z|X; \eta)} \\ &\quad + \langle \log p_\rho(Z'|Z) \rangle_{\pi(X)q(Z|X; \eta) q_T(\tilde{X}|X; u_A) q(Z'|\tilde{X}; \eta)} \\ &\quad - \left\langle \log q(Z'|\tilde{X}; \eta) \right\rangle_{\pi(X)q(Z|X; \eta) q_T(\tilde{X}|X; u_A) q(Z'|\tilde{X}; \eta)} \\ &\quad - \left\langle \log q_T(\tilde{X}|X; u_A) \right\rangle_{\pi(X)q_T(\tilde{X}|X; u_A)} \quad (23) \end{aligned}$$

The objective is

$$(\eta^*, \theta^*) = \arg \max_{\eta, \theta} \min_{u_A \in \mathcal{U}_A} \tilde{\mathcal{B}}_{\text{SE}}(\theta, \eta; u_A) \quad (24)$$

Iterative optimization for $\tau = 1, 2, \dots$:

- Augmentation step: Solve or improve $u_A^{(\tau)} = \arg \min_{u_A \in \mathcal{U}_A} \tilde{\mathcal{B}}_{\text{SE}}(\theta^{(\tau-1)}, \eta^{(\tau-1)}; u_A)$
- Maximization step: Solve or improve $(\eta^{(\tau)}, \theta^{(\tau)}) = \arg \max_{\eta, \theta} \tilde{\mathcal{B}}_{\text{SE}}(\theta, \eta; u_A^{(\tau)})$

Augmentation step: In the inner optimization we seek for the worst case u_A that will minimize the ELBO, or equivalently

$$u_A^* = \arg \min_{u_A \in \mathcal{U}_A} \left\{ \tilde{\mathcal{B}}_{\text{SE}}(\theta, \eta; u_A) \right\}$$

While this optimization seems to be on the space of all distributions, we can see that the last term (23) of the bound $\tilde{\mathcal{B}}_{\text{SE}}$ is the entropy of q_T , $H[q_T]$. Consequently, the bound $\tilde{\mathcal{B}}_{\text{SE}}$ is minimized when the entropy $H[q_T]$ is minimized, i.e. when q_T is degenerate, and concentrated on a point. Consequently, focusing on the remaining terms we can rewrite this optimization problem for each data point as

$$\alpha^* = \arg \max_{\alpha \in A} \left\{ - \langle \log p(Z'|Z; \rho) \rangle_{q(Z|X=x; \eta) q(Z'|\tilde{X}=T_\alpha(x); \eta)} \right. \quad (25)$$

$$\left. - H[q(Z'|\tilde{X} = T_\alpha(x); \eta)] - H[q(Z|X = x; \eta)] \right\} \quad (26)$$

$$\tilde{x}_a = x + \alpha^* \quad (27)$$

This term can be identified as a lower bound to the entropy regularized ℓ_2 optimal transport [5] hence is measuring the discrepancy between $q(Z|X = x; \eta)$ and $q(Z'|\tilde{X} = \tilde{x}; \eta)$. It can be interpreted as an adversarial attack trying to maximize the change in the representations. We will denote the empirical distribution that is obtained by attacking each sample adversarially as $\hat{\pi}_a(\tilde{X}|X) = \sum_i \delta(\tilde{X} - \tilde{x}_a^{(i)})$.

Maximization step: Given the empirical distribution of inputs and their augmentation via adversarial attacks, denoted as $\hat{\pi}_a(X, \tilde{X}) \equiv \pi(X)\hat{\pi}_a(\tilde{X}|X)$ is fixed in an iteration, the objective is

$$\begin{aligned}
\tilde{B}_{\text{SE}}(\theta, \eta) &= + \langle \log p(X|Z; \theta) \rangle_{\pi(X)q(Z|X; \eta)} \\
&\quad + \langle \log p(Z) \rangle_{\pi(X)q(Z|X; \eta)} \\
&\quad - \langle \log q(Z|X; \eta) \rangle_{\pi(X)q(Z|X; \eta)} \\
&\quad + \langle \log p_\rho(Z'|Z) \rangle_{q(Z|X; \eta)q(Z'|\tilde{X}; \eta)\hat{\pi}_a(X, \tilde{X})} \\
&\quad - \langle \log q(Z'|\tilde{X}; \eta) \rangle_{q(Z|X; \eta)q(Z'|\tilde{X}; \eta)\hat{\pi}_a(X, \tilde{X})} \\
&= \langle \log p(X|Z; \theta) \rangle_{\pi(X)q(Z|X; \eta)} \\
&\quad - \mathcal{KL}(\hat{\pi}_a(X, \tilde{X})q(Z, Z'|X, X'; \eta) \| p_\rho(Z', Z))
\end{aligned} \tag{28}$$

where $q(Z, Z'|X, X'; \eta) \equiv q(Z|X; \eta)q(Z'|\tilde{X}; \eta)$.

C.3.1 A Tighter bound

Even though we derived the above bound using a factorized distribution assumption $q(Z, Z'|X, X'; \eta) = q(Z|X; \eta)q(Z'|\tilde{X}; \eta)$, [5] is using a tighter bound using

$$q(Z', Z|X = x, \tilde{X} = \tilde{x}; \eta) = \mathcal{N} \left(\begin{pmatrix} f^\mu(x; \eta) \\ f^\mu(\tilde{x}; \eta) \end{pmatrix}, \begin{pmatrix} f^\Sigma(x; \eta) & \psi \\ \psi & f^\Sigma(\tilde{x}; \eta) \end{pmatrix} \right)$$

Here, ψ is a diagonal matrix with the i 'th diagonal element

$$\psi_i = \frac{1}{2\gamma} \left(\sqrt{1 + 4\gamma^2 f^\Sigma(x; \eta)_i f^\Sigma(\tilde{x}; \eta)_i} - 1 \right)$$

where $\gamma \equiv \rho/(1 - \rho^2)$. With this modification we get

$$\begin{aligned}
\langle \log p_\rho(Z', Z) \rangle_{\tilde{q}(Z', Z|X=x, \tilde{X}=\tilde{x}; \eta)} &= -\frac{1}{1 - \rho^2} (f^\mu(x; \eta) + f^\Sigma(x; \eta) + f^\mu(\tilde{x}; \eta) + f^\Sigma(\tilde{x}; \eta)) \\
&\quad + \frac{2\rho}{1 - \rho^2} (\psi + f^\mu(x; \eta)f^\mu(\tilde{x}; \eta)) + C
\end{aligned} \tag{29}$$

Under the q distribution, the desired expectations are

$$\langle \text{Tr} Z' Z'^\top \rangle = \text{Tr}(\tilde{\Sigma} + \tilde{\mu}\tilde{\mu}^\top) \quad \langle Z Z^\top \rangle = \text{Tr}(\Sigma + \mu\mu^\top) \quad \langle Z' Z'^\top \rangle = \text{Tr}(\psi + \tilde{\mu}\tilde{\mu}^\top) \tag{30}$$

$\mu \equiv f^\mu(x; \eta)$, $\tilde{\mu} \equiv f^\mu(\tilde{x}; \eta)$, $\Sigma \equiv f^\Sigma(x; \eta)$, $\tilde{\Sigma} \equiv f^\Sigma(\tilde{x}; \eta)$

$$\langle \log p_\rho(Z', Z) \rangle_{\tilde{q}} = -\frac{1}{2(1 - \rho^2)} \text{Tr} \left(\tilde{\Sigma} + \Sigma + \tilde{\mu}\tilde{\mu}^\top + \mu\mu^\top - 2\rho(\psi + \tilde{\mu}\tilde{\mu}^\top) \right) \tag{31}$$

With the given tighter bound the algorithm for SE is shown in Algorithm 2. From Equation 18 we approximate the required expectations by their Monte Carlo estimates and the objective function to maximize becomes

$$\begin{aligned}
\hat{B}_{\text{SE}}(\theta, \eta; x, \tilde{x}, z) &= \langle \log p(X = x|Z = z) \rangle_{q(Z|X=x; \eta)} \\
&\quad + \langle \log p(Z', Z) \rangle_{\tilde{q}(Z, Z'|X=x, \tilde{X}=\tilde{x})} \\
&\quad - \langle \log \tilde{q}(Z, Z') \rangle_{\tilde{q}(Z, Z'|\tilde{X}=\tilde{x}, X=x)}
\end{aligned} \tag{32}$$

C.4 AVAE-SS (Self Supervised)

This algorithm can be used for post training an already trained VAE. Figure 6 shows the graphical model describing AVAE-SS model.

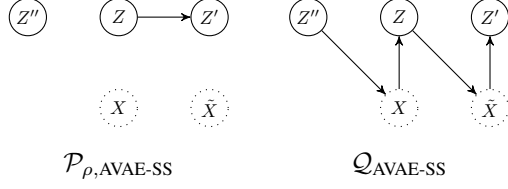


Figure 6: Graphical model of the AVAE-SS target distribution $\mathcal{P}_{\rho, \text{AVAE-SS}}$, and the variational approximation $\mathcal{Q}_{\text{AVAE-SS}}$. Here both X and \tilde{X} is a sample generated by the decoder.

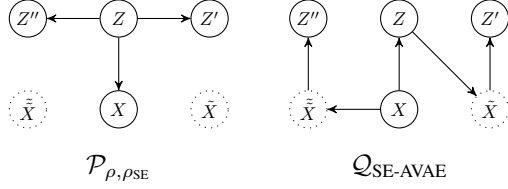


Figure 7: Graphical model of the target distribution $\mathcal{P}_{\rho, \rho\text{SE}}$, and the variational approximation $\mathcal{Q}_{\text{SE-AVAE}}$. Here \tilde{X} is a sample generated by the decoder that is subsequently encoded by the encoder.

$$\begin{aligned}
\mathcal{B}_{\text{AVAE-SS}} &= + \quad -\mathcal{KL} \left(p(Z'')p(X|Z'')q(Z|X; \eta)p(\tilde{X}|Z)q(Z'|\tilde{X}) \parallel p(Z'')p(Z'|Z)p(Z)u(\tilde{X})u(X) \right) \\
&= \langle \log p(Z) \rangle_{q(Z|X)} + \langle \log p(Z'|Z) \rangle_{q(Z|X)q(Z'|\tilde{X})} \\
&\quad - \left\langle \log p(Z'')p(X|Z'')q(Z|X; \eta)p(\tilde{X}|Z)q(Z'|\tilde{X}) \right\rangle_{p(X|Z'')q(Z|X; \eta)p(\tilde{X}|Z)q(Z'|\tilde{X})} \quad (33)
\end{aligned}$$

The algorithm is shown in Algorithm 4. We approximate the required expectations by their Monte Carlo estimates and the objective function to maximize becomes

$$\begin{aligned}
\hat{\mathcal{B}}_{\text{AVAE-SS}}(\theta, \eta; x, \tilde{x}, z) &= \langle \log p(Z) \rangle_{q(Z|X=x; \eta)} + \langle \log p(Z'|Z; \rho) \rangle_{\tilde{q}(Z|X=x; \eta)\tilde{q}(Z'|\tilde{X}=\tilde{x}; \eta)} \\
&\quad - \left\langle \log q(Z'|\tilde{X}=\tilde{x}; \eta) \right\rangle_{q(Z'|\tilde{X}=\tilde{x}; \eta)} \\
&\quad - \langle \log q(Z|X=x; \eta) \rangle_{q(Z|X=x; \eta)} \quad (34)
\end{aligned}$$

Also see Section C.1 for further expansion on terms.

C.5 SE-AVAE

Figure 7 shows the graphical model describing AVAE-SS model.

$$\begin{aligned}
\mathcal{B}_{\text{SE-AVAE}} &= + \quad -\mathcal{KL}(\pi(X)p(\tilde{X}|X)q(Z''|\tilde{X}; \eta)q(Z|X)p(\tilde{X}|Z; \eta)q(Z'|\tilde{X}) \\
&\quad \parallel p(Z'|Z)p(Z''|Z)p(X|Z)p(Z))
\end{aligned}$$

The algorithm is shown in Algorithm 3. We approximate the required expectations by their Monte Carlo estimates and the objective function to maximize becomes

$$\begin{aligned}
\hat{\mathcal{B}}_{\text{SE-AVAE}}(\theta, \eta; x, \tilde{x}, \tilde{\tilde{x}}, z) &= \langle \log p(Z) \rangle_{q(Z|X=x; \eta)} + \langle \log p(Z'|Z; \rho) \rangle_{\tilde{q}(Z|X=x; \eta)\tilde{q}(Z'|\tilde{X}=\tilde{x}; \eta)} \\
&\quad + \langle \log p(Z''|Z; \rho_{\text{SE}}) \rangle_{\tilde{q}(Z|X=x; \eta)\tilde{q}(Z''|\tilde{\tilde{X}}=\tilde{\tilde{x}}; \eta)} \\
&\quad - \left\langle \log q(Z'|\tilde{X}=\tilde{x}; \eta) \right\rangle_{q(Z'|\tilde{X}=\tilde{x}; \eta)} \\
&\quad - \langle \log q(Z|X=x; \eta) \rangle_{q(Z|X=x; \eta)} \\
&\quad - \left\langle \log q(Z''|\tilde{\tilde{X}}=\tilde{\tilde{x}}; \eta) \right\rangle_{q(Z''|\tilde{\tilde{X}}=\tilde{\tilde{x}}; \eta)} \quad (35)
\end{aligned}$$

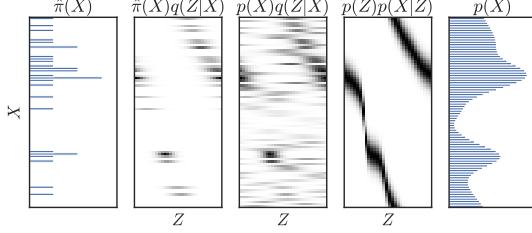


Figure 8: Results of a VAE. (Left to right) i) The empirical data distribution $\hat{\pi}(X)$, ii) Encoder weighted by the empirical distribution $\hat{\pi}(X)q(Z|X; \eta)$, iii) Encoder weighted by the model distribution $p(X; \theta)q(Z|X; \eta)$, iv) the decoder $p(X|Z)p(Z)$, v) the model distribution $p(X; \theta)$, obtained by marginalizing the decoder.

D Details of the 1-D Example

In this example Section 3.1, we will assume that both the observations x and latents z can only take values from discrete sets and to avoid boundary effects we adopt a parametrization reminiscent of a von-Mises distribution with normalization constant J :

$$\mathcal{VM}(X; \mu, v) \equiv \frac{1}{J(\mu, v)} \exp(\cos(X - \mu)/v) \quad J(\mu, v) = \sum_{x \in \mathcal{X}} \exp(\cos(X - \mu)/v)$$

As these densities (up to quantization effects) are unimodal and symmetric around their means with a bell-shape, this example is qualitatively similar to a standard conditionally Gaussian VAE. We define the following system of conditional distributions as the decoder and encoder models as:

$$p(X|Z = z; \theta) = \mathcal{VM}(X; g(z; \theta), v) \quad q(Z|X = x; \eta) = \mathcal{VM}(Z; f^\mu(x; \eta), f^\Sigma(x; \eta))$$

where we let $X \in \{c_x, 2c_x, 3c_x, \dots, N_x c_x\}$, with $c_x = 2\pi/N_x$ and $Z \in \{c_z, 2c_z, 3c_z, \dots, N_z c_z\}$, with $c_z = 2\pi/N_z$ where N_x and N_z are the cardinalities of each set. As both X and Z are discrete we can store g, f^μ, f^Σ as tables, hence the trainable parameters are just the function values at each point $\theta = (g_1, \dots, g_{N_z})$ and $\eta = (\mu_1, \dots, \mu_{N_x}, \sigma_1, \dots, \sigma_{N_x})$. This emulates a high capacity network that can model any functional relationship between latents and observations. The prior $p(Z)$ is chosen as uniform and the coupling term is

$$p(Z'|Z = z) = \mathcal{VM}(Z'; z, \nu_\rho)$$

where the spread term ν_ρ is chosen on the order of 10^{-3} .

In Figure 8, we illustrate an example where we fit a VAE to the empirical data distribution $\hat{\pi}(X)$. The encoder-empirical data joint distribution $\hat{\pi}(X)q(Z|X; \eta)$ and the decoder joint distribution $p(X|Z)p(Z)$ are in fact closely matching but only on the support of $\hat{\pi}$. In the next panel, we show the encoder-model data joint distribution $p(X; \theta)q(Z|X; \eta)$. The nonsmooth nature of the encoder is evident, conditional distributions at each row are quite different from one other. This reveals that samples that can be still generated with high probability with the decoder would be mapped to unrelated states when encoded again.

E Wasserstein Distance

The ℓ_2 -Wasserstein distance \mathcal{W}_2 between two Gaussians P_a and P_b with means μ_a, μ_b and covariance matrices Σ_a, Σ_b is given by

$$\mathcal{W}_2^2(P_a, P_b) \equiv \|\mu_a - \mu_b\|_2^2 + \text{Tr}(\Sigma_a + \Sigma_b - 2(\Sigma_b^{1/2}\Sigma_a\Sigma_b^{1/2})^{1/2})$$

F Experimental Details

All experiments are performed on NVIDIA Tesla P100 GPU. Optimization is performed using AdamOptimizer with learning rate $1e-4$.

Color Mnist For experiments with the Color MNIST dataset with MLP architecture, a 4 layer multi layer perceptron (MLP), with 200 neurons at each layer, is used for both encoder and decoder. For experiments with the Color MNIST dataset and conv architecture, a 7 layer VGG network is used for

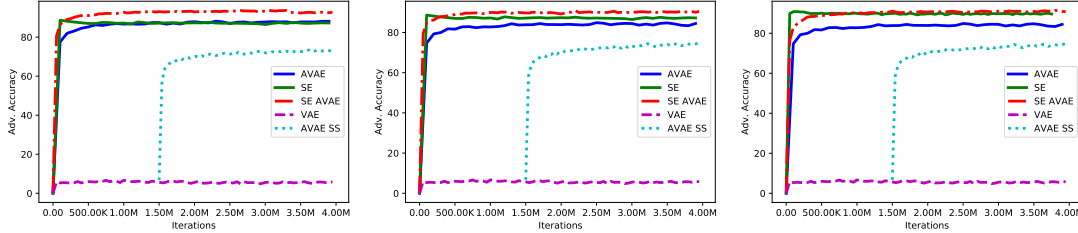


Figure 9: Comparison of Algorithms (on ColorMnist with Conv arch) for various different ρ and ρ_{SE} values. (LEFT) $\rho = 0.95$ and $\rho_{SE} = 0.975$. (MIDDLE) $\rho = 0.97$ and $\rho_{SE} = 0.97$. (RIGHT) $\rho = 0.97$ and $\rho_{SE} = .975$

encoder with number of output channels 8, 16, 32, 64, 128, 256 and 512 respectively with strides 2, 1, 2, 1, 2, 1 and 2 respectively and kernel shape of (3, 3). For decoder a de-convolutional architecture 3 de-conv layers with output channels 64, 32 and 3, strides 1, 2 and 1, and kernel shape (3, 3) is used. Convolutional architectures are stabilized using BatchNorm between each convolutional layer. In training where adversarial attack is required, PGD with L-inf perturbation radius and iteration budget 20 is used. In PGD no random restarts are used for training, while evaluating 10 random restarts are used. In evaluation, PGD with iteration budget 40 is used.

CelebA CelebA experiments are performed using VGG encoder with 4 convolutional layers, output channels 128, 256, 512, and 1024 respectively, stride 2 and kernel size (5, 5). CelebA decoder is VGG network with 4 layers, output channels 512, 256, 128 and 3, stride 2 and kernel shape (5, 5). All convolutional layers are normalized with BatchNorm. In training where adversarial attack is required, PGD attack with iteration budget 5 is used with L-inf perturbation radius. In training no random restarts are used in PGD where as in evaluation 10 random restarts are used with 20 iteration budget.

G Comparing Algorithms for different ρ settings

Figure 9 shows comparison of all algorithms for different ρ and ρ_{SE} values. Figure solidifies the claim that SE-AVAE achieves better downstream adversarial accuracy than both SE and VAE, for smaller ϵ values for reasonable ρ and ρ_{SE} values.

H CelebA Results for All Downstream Tasks

Table 3 shows adversarial downstream accuracy for all 17 downstream tasks of CelebA, compared across models VAE, AVAE, SE with 5 PGD iteration budget, SE with 20 PGD iteration budget, SE AVAE and AVAE SS. Here $\epsilon = 0.0$ represents the nominal downstream accuracy.

Task	VAE		AAVE		SE ⁵		SE ²⁰		SE AVE		AAVE SS	
	0.0	0.1	0.0	0.1	0.0	0.1	0.0	0.1	0.0	0.1	0.0	0.1
Bald	97.9	2.1	97.8	83.9	97.9	71.0	97.4	86.5	97.8	87.0	97.8	70.0
Mustache	94.9	0.7	94.8	89.8	95.0	69.5	95.7	84.4	96.3	92.3	95.2	74.0
Eyeglasses	95.4	0.0	94.9	71.7	95.9	20.3	95.7	33.0	95.3	67.5	94.3	56.8
Necklace	87.7	0.7	88.2	76.7	88.0	56.0	88.0	78.9	86.1	80.3	87.9	59.9
Smiling	87.7	0.4	78.5	3.0	86.9	3.1	85.7	1.1	77.9	6.3	81.6	1.0
Lipstick	84.5	0.0	80.4	6.5	84.5	2.0	80.3	0.6	80.7	11.2	80.3	0.9
Bangs	90.3	0.2	89.7	36.0	90.8	19.3	89.6	27.0	89.6	45.9	89.6	22.2
Black Hair	83.5	0.0	82.5	31.7	83.4	23.0	81.4	31.4	79.5	33.3	83.3	26.2
Blond Hair	91.5	0.2	91.1	46.4	92.5	35.9	90.7	53.5	92.4	55.8	90.6	37.6
Brown Hair	78.4	1.0	77.8	35.9	77.9	24.1	80.5	41.5	82.9	46.0	78.2	19.3
Gender	87.6	0.0	82.6	5.4	87.8	1.5	81.6	0.7	82.1	10.7	82.1	0.7
Beard	85.8	0.0	83.8	39.2	85.4	18.3	85.3	24.3	86.0	50.1	84.4	16.3
Straight Hair	79.6	2.3	79.2	72.2	79.6	64.8	78.7	77.3	78.8	74.9	79.2	64.8
Wavy Hair	75.8	0.1	75.8	17.8	76.1	10.0	72.8	10.2	72.7	22.1	75.5	9.3
Earrings	81.3	0.1	81.0	60.9	81.0	26.8	81.3	55.3	79.5	64.1	81.2	24.7
Hat	96.5	0.2	96.6	75.2	96.9	55.3	96.4	77.3	97.3	82.7	96.0	65.5
Necktie	92.6	0.2	92.5	61.9	92.7	41.0	92.7	51.7	93.0	72.5	92.6	39.8
Time Factor	×1		×2.2		×3.1		×7.8		×4.3		×2.2	
MSE	7203.9		7276.6		7208.8		N/A		7269.2		7347.3	
FID	99.86		97.92		98.00		N/A		109.4		99.86	

Table 3: Adversarial test accuracy (in percentage) of the representations for all of classification tasks on CelebA.